A proprioceptive mechanism for bioinspired fish swimming

J. Sánchez-Rodríguez,[1] F. Celestini,[1] C. Raufaste,[1,2] and M. Argentina[1]

[1] *Université Côte d'Azur, CNRS, Institut de Physique de Nice, 06100 Nice, France*
[2] *Institut Universitaire de France (IUF)*

(Dated: March 23, 2021)

In this letter, we propose a mechanism for driving bioinspired fish swimming locomotion based on proprioceptive sensing. Proprioception provides information about and representation of a body's position, motion and acceleration in addition to the usual five senses. We hypothesize that a feedback loop based on this "sixth" sense results in an instability, driving the locomotion. In order to test our assumptions, we use a biomimetic robot and compare the experimental results to a simple yet generic model, with excellent agreement.

Multicellular organisms exhibit tremendous diversity in physiology and shape. This variety is usually rationalized by the adaption to their environment within the Darwinian evolution, but also by the functions needed by the animals to live [1]. Locomotion is among the mandatory functions, motivating physicists to study it, as motions result from a mechanical interaction of the organism with its environment. There is a huge variation of gaits in animals for achieving locomotion [2]. However, we expect general mechanisms to be at play because all the movements result from mechanical principles.

Almost all known vertebrates are equipped with Central Pattern Generators (CPG) [3, 4]. CPG are neural networks that are able to provide a rhythmic output without any external driving and that control locomotion. Nevertheless, CPG are tuned with sensory feedback, because the motion must be obviously adapted to the environment of the moving organism [5]. Sensory information encompasses the traditional five senses as well as proprioception which is the sense of self-movement or body position. This last class of sensing is usually responsible for the adaptation of the rhythmic driving of the muscles [6, 7] and suggests that locomotion is driven through proprioceptive feedback as sketched in Fig. 1.

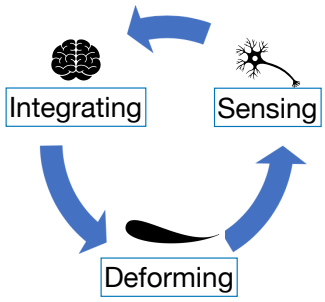

FIG. 1. Proprioception scheme: the extension of the muscles providing the deformation is moderated by the integration of the information from the proprioceptive sensors.

Predicting the swimming gaits has been the subject of a variety of studies for more than half a century [8–14]. In all these studies, the kinematics of the swimmer was imposed and predictions for the selected tail-beat amplitude and frequency remained very limited. It is only recently that the proprioceptive loop depicted in Fig. 1 was hypothesized to drive the dynamics of the fish deformation [15, 16] and led to the development of the first numerical models [17, 18]. In addition, fish-like robotic systems have proven to be very efficient underwater vehicles from early attempts [19, 20] to very advanced prototypes [21–23]. Their ability to probe the environment [24–26] or their own deformation [27] opens the route towards fully autonomous artificial swimmers in the near future as also observed with quadrupedal robots for terrestrial locomotion [28].

In this letter, we propose the first demonstration of swimming following the simple scheme shown in Fig. 1 using a robotic fish which undulates in a thunniform way. Based on information collected by a force sensor, this proprioceptive robot swims without any input from an operator (movie in Supplemental Material [29]). We show that the activation of the robot is ensured by an oscillatory instability, whose threshold matches the environment: the robot does not move in air as it does in water. This general mechanism opens a new route towards the development of autonomous underwater vehicles.

The robotic fish was described in a former study [22]. Its soft tail and fin are 3D printed using a flexible polymer ("Ninjaflex" filament from NinjaTek). Two cables attached to the end of the tail are actuated by the wheel of a waterproof servomotor (Hitec HS-5086WP), and permit the bending of the tail, as seen in Fig. 2, whose deformation is quantified by the angle α defined from the position of a tracer located in the middle of the fin. The servomotor is attached to a force sensor (RFS 150 XY from Honigmann), which measures the two components F_x and F_y of the force exerted by the fluid on the swimmer, respectively aligned and normal to the swimming direction. We use F_y as the proprioceptive information to trigger locomotion. The servomotor wheel angle is denoted ϕ and follows the instruction angle ϕ_c:

$$\phi_c = -\gamma F_y \quad (\textbf{Integrating stage} \text{ in Fig. 1}), \qquad (1)$$

where γ is the control parameter of the proprioceptive driving. In water, it appears that above the critical threshold $\gamma_{c,\mathrm{exp}} \sim 0.72$ rad.N^{-1}, the robotic tail undergoes spontaneous oscillations with a very well defined angular peak-to-peak amplitude α_0 and frequency ω. In

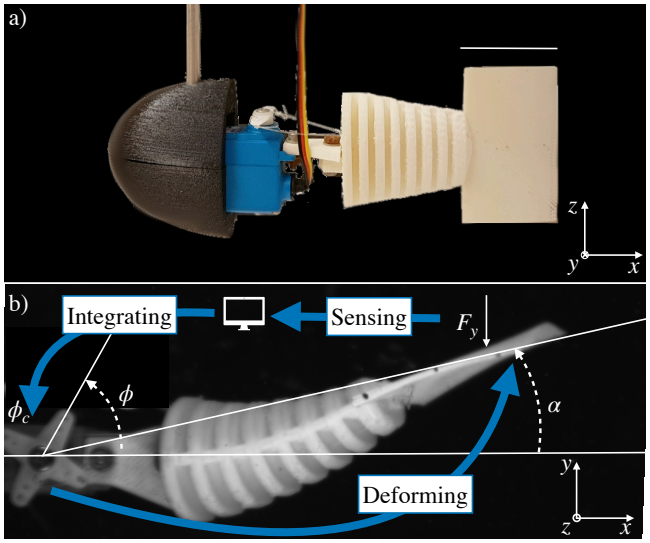

FIG. 2. a) Side view of the fish-like robotic system: the white material is 3D printed using soft polymers. The tail is driven by two cables attached to a waterproof servomotor (blue piece). The swimmer is attached to a force sensor (vertical rod connected to the head). The thin white bar represents 3.5 cm. b) Top view of the servomotor and the elastic tail.

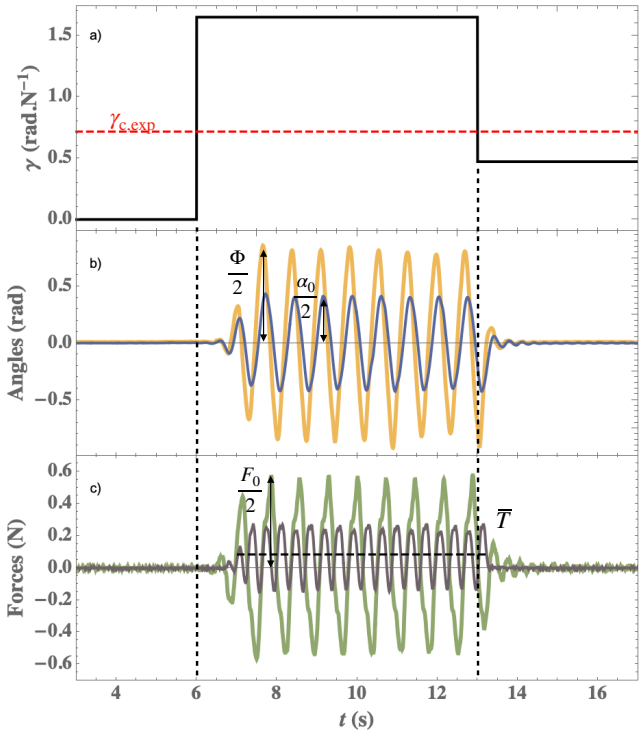

FIG. 3. a) A typical temporal variation on the feedback parameter γ. b) The dynamics of the angles α (blue) and ϕ (orange), as the controlling parameter γ is varied. The angular frequency ω is deduced from the period $2\pi/\omega$. c) Temporal evolution of the lateral force F_y (green) and of the thrust $T = -F_x$ (grey) with F_x the longitudinal force. We also show the mean thrust $\overline{T}$ in steady state for $\gamma = 1.65$ rad.N^{-1} (dashed horizontal line). α_0, Φ_0 and F_0 denote the peak-to-peak amplitudes of $\alpha(t)$, $\phi(t)$ and $F_y(t)$ respectively. Movie in Supplemental Material [29].

Fig. 3, we present the typical temporal evolution of the angles (ϕ and α) and forces ($T = -F_x$ and F_y), as the controlling parameter γ is varied. For $\gamma < \gamma_{c,\mathrm{exp}}$, the system is stable, and no locomotion is expected. Nevertheless, as $\gamma > \gamma_{c,\mathrm{exp}}$, an instability occurs and leads to a periodic undulation of the tail. This oscillation induces a non-zero mean thrust $\overline{T} = -\overline{F}_x > 0$, which indicates the capacity of the proprioceptive loop to induce locomotion. The oscillation amplitude increases with γ and the frequency is of order $\omega \sim 10$ s^{-1}, as seen in Fig. 4.

We propose a simple, yet generic, model to shed light on the instability and discuss how it relies on the **sensing information** of the feedback loop depicted in Fig 1. We first assume that the tail undulates with a relatively small amplitude and we consider $\alpha \ll 1$. In this limit, F_y depends on α and on its temporal derivatives:

$$F_y = -K_{\ddot{\alpha}}\ddot{\alpha} - K_{\dot{\alpha}}\dot{\alpha} - K_{\alpha}\alpha \quad (\textbf{Sensing stage}), \qquad (2)$$

where $K_{\ddot{\alpha}}$, $K_{\dot{\alpha}}$, K_{α} and $K_{\dot{\alpha}^2}$ are parameters characterizing the medium, the material or the substrate with which the swimmer interacts and could by construction account for inertial, viscous, elastic effects. During the motion of a fish at velocity U in a fluid at high Reynolds numbers, a simple scaling analysis recovers the terms found by Theodorsen in his theory of oscillating airfoils [30]:

$$K_{\ddot{\alpha}} \sim \rho L^4, \; K_{\dot{\alpha}} \sim \rho U L^3, \; K_{\alpha} \sim \rho U^2 L^2, \qquad (3)$$

with ρ the density of the fluid (here 1000 kg.m^{-3} for water) and $L = 10$ cm, the typical length of the fish. The first term $K_{\ddot{\alpha}}$ accounts for the added mass due to the bolus of water accelerated during the tail oscillation, while the last two terms account for the lift of a moving and inclined airfoil in a flow. To guess which term is dominant, we compute the ratios $K_{\ddot{\alpha}}\ddot{\alpha}/(K_{\dot{\alpha}}\dot{\alpha}) \sim \omega^\star$ and $K_{\ddot{\alpha}}\ddot{\alpha}/(K_{\alpha}\alpha) \sim \omega^{\star 2}$, where we have introduced the dimensionless number $\omega^\star = \omega L/U$. It appears that for biological swimmers, this dimensionless parameter is large [31], $\omega^\star \sim 10$, and this is also verified in our experiments. Hence, only the first term in the expansion (2) should be kept in Theodorsen's framework. However, experiments detailed in Supplemental Material [29] performed without external flow, $U = 0$, and with an imposed harmonic forcing around the angular frequencies of interest, give precise measurements of $K_{\ddot{\alpha}} = (11.3 \pm 0.1)$ mN.rad^{-1}.s^2 and $K_{\dot{\alpha}} = (147 \pm 1)$ mN.rad^{-1}.s^1. As a consequence, $K_{\ddot{\alpha}}\ddot{\alpha}/(K_{\dot{\alpha}}\dot{\alpha}) \simeq \omega K_{\ddot{\alpha}}/K_{\dot{\alpha}} \sim 1$ around $\omega \sim 10$ s^{-1} and $K_{\dot{\alpha}}\dot{\alpha}$ cannot be discarded in the force expression even if $U = 0$. We interpret this term as a viscous force due to the oscillation of the tail inside a fluid of viscosity η, 1 mPa.s for water. By comparing with the case of a cylinder of radius and length L [32], this leads to a rough estimate of $K_{\dot{\alpha}} = 2\pi L^3\sqrt{2\rho\eta\omega} \sim 30$ mN.rad^{-1}.s, in agreement with the precise measurement mentioned.

Note that given the relatively high value of the Reynolds number based on the transverse motion of the plate, $\rho\alpha_0 L^2\omega/\eta \sim 10^4$, nonlinear terms could be expected as a transverse pressure drag force writing $-c_y\rho L^4|\dot{\alpha}|\dot{\alpha}$, with c_y a dimensionless coefficient. Experimentally we expect $c_y \ll 1$ since we do not observe any significant frequency doubling in the temporal signal of the transverse force F_y (Fig. 3c) and the amplitude of the force is proportional to the amplitude of the harmonic forcing (Fig. S4 in Supplemental Material [29]). As discussed in [32], convective terms in Navier-Stokes equation can be dominated by unsteady terms in oscillatory flow. This could explain the prevalence of the linear term in $\dot{\alpha}$. Nevertheless, accounting for this nonlinear term improves the matching between the model and the experimental data at high α_0 values as described in Supplemental Material [29].

For consistency with what follows, we re-write

$$F_y = -K_{\ddot{\alpha}}\left(\ddot{\alpha} + \xi\omega_0\dot{\alpha}\right), \tag{4}$$

with ξ a dimensionless factor and ω_0 a quantity that has the dimension of a frequency.

We now show that the **deforming stage** in Fig. 1, quantified by the tail angle $\alpha(t)$, can be predicted by the dynamics of a weakly nonlinear oscillator driven by the servomotor. By exploiting the momentum balance applied to the tail along the y-axis, we write

$$m_t L\ddot{\alpha} = F_y + F_d, \tag{5}$$

with m_t the mass of the tail, F_y the fluid-structure interaction force characterized in Eq. 4 and F_d the driving force in the y-direction. The latter has to fulfill two conditions: first it drives the angle α with respect to the control angle $\alpha^\star(t) = K_1\phi(t)$, where $K_1 = 0.55$ is a parameter measured in quasistatic experiments [29]. Second, at the leading order deformation, F_d is modeled by a polynomial function of $\delta\alpha = \alpha - \alpha^\star$, without a quadratic monomial due to the symmetry of the problem. This nonlinear function captures the shift of the resonance frequency with the amplitude as observed with the robotic fish [22] or flexible panels in other setups [33–36]. Consequently, we write $F_d(t) \propto -\delta\alpha(t)\left[1 - K_2\delta\alpha(t)^2\right]$, with K_2 a parameter that weights the nonlinear term with respect to the linear one. Given that $K_{\ddot{\alpha}} \sim \rho L^4$ and that fish in general, and the robotic fish in particular, are slender objects [37], we expect $m_t \ll \rho L^3$ and the dynamical equation 5 becomes:

$$\ddot{\alpha} + \xi\omega_0\dot{\alpha} + \omega_0^2(\alpha - K_1\phi)\left[1 - K_2(\alpha - K_1\phi)^2\right] = 0, \tag{6}$$

with ω_0 now interpreted as the linear regime oscillation frequency of the tail around its equilibrium value $K_1\phi$. In addition, ξ is interpreted as the damping factor of the oscillator.

To close the system, we now model the response of the servomotor to account for the error between the instruction angle ϕ_c and the output angle ϕ associated with this element in the proprioceptive loop. In Supplemental Material [29], we show that the dynamics is mainly limited by the finite angular velocity Ω of the servomotor wheel and is well described by

$$\dot{\phi} = \Omega\tanh\left(\frac{\phi_c - \phi}{\Delta\phi}\right), \tag{7}$$

where the parameter $\Delta\phi$ represents the typical angle difference between the instruction and the wheel angle at which the servomotor achieves maximum velocity.

In the Supplemental Material [29], we describe the experimental methods to measure the values of the various parameters involved in the feedback loop; they are summarized in Tab. I. The set composed of the fluid

TABLE I. Measured parameters

ω_0	ξ	Ω	$\Delta\phi$	K_1	K_2	$K_{\ddot{\alpha}}$
13.0	1.0	7.0	0.26	0.55	1.6	11.3
s^{-1}		$rad.s^{-1}$	rad		rad^{-2}	$mN.rad^{-1}.s^2$

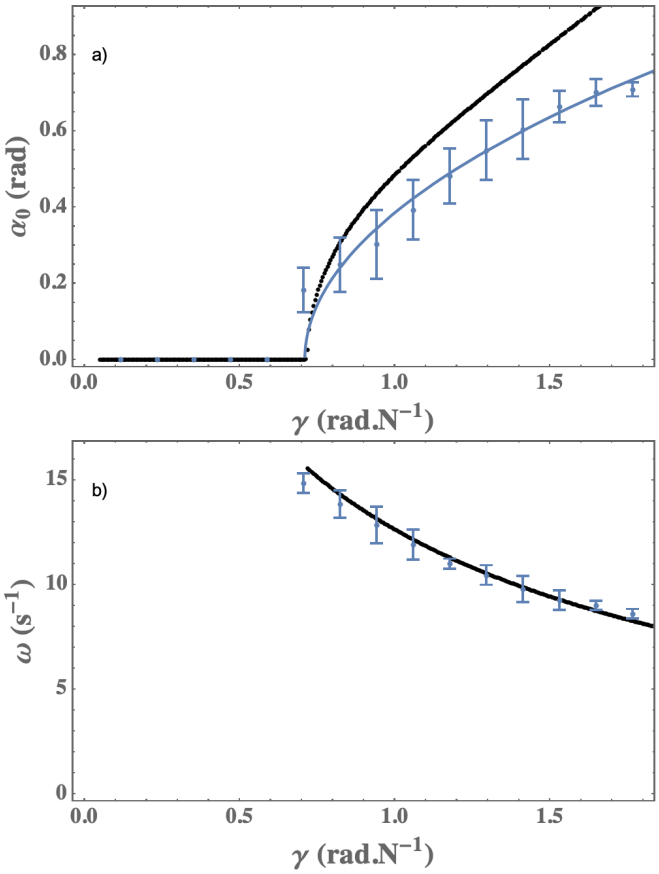

FIG. 4. Oscillatory characteristics of the proprioceptive loop. a) Angular amplitude of the tail oscillation α_0 as a function of γ. b) Angular frequency ω as a function of γ. The experimental measurements and their error bars are drawn in blue. In a), the thin blue curve passing through the data is an interpolation with the function $\alpha_0 = \Theta_{\text{exp}}\sqrt{\gamma - \gamma_{\text{c,exp}}}$ with $\gamma_{\text{c,exp}} = 0.72$ rad.N^{-1} and $\Theta_{\text{exp}} = 0.72$ rad$^{1/2}$N$^{1/2}$. The numerical predictions are represented by thick black lines.

force relation (4) coupled to equations (1,6,7) constitutes a generic model for proprioceptive locomotion. This system has a steady solution $\alpha = \phi = 0$, which corresponds to a nonmoving swimmer. Our conjecture is that an oscillatory instability is responsible for the proprioceptive locomotion. Following this idea, we perform a standard linear stability analysis around the stationary state. We find an oscillatory instability related to a Hopf bifurcation [38] at $\gamma = \gamma_c$. From a dimensional analysis, we expect $\gamma_c \propto (K_{\ddot{\alpha}}\omega_0^2)^{-1}$ with a proportionality constant that depends on the dimensionless parameters K_1, ξ and $\frac{\Omega}{\omega_0 \Delta\phi}$. The full calculation gives

$$\gamma_c = \frac{2\xi + \frac{\omega_0 \Delta\Phi}{\Omega}\left(1 + \xi^2 - \sqrt{1 + 4\xi\frac{\Omega}{\omega_0\Delta\Phi} - 2\xi^2 + \xi^4}\right)}{2\xi K_1 K_{\ddot{\alpha}} \omega_0^2}, \tag{8}$$

which creates an oscillation of frequency ω_c at threshold

$$\omega_c = \omega_0 \sqrt{\frac{(1-\xi^2)}{2}} \sqrt{1 + \sqrt{1 + 4\frac{\Omega}{\Delta\phi\omega_0}\frac{\xi}{(1-\xi^2)^2}}}. \tag{9}$$

From the values of the parameters (Tab. I), we found the predicted threshold value for γ to be $\gamma_c \sim 0.75$ rad.N^{-1} and the oscillation frequency to be $\omega_c \sim 15.6$ rad.s^{-1}. The agreement is very satisfactory given there is no free parameter once the physical model parameters are measured.

Using a fourth-order Runge-Kutta algorithm, we have numerically integrated the complete nonlinear system, and we compare the model prediction with the experimental measurements in Fig. 4. It appears that both the oscillation angular amplitude and frequency in experiments are well captured by the simple model, taking into account again that there is no free parameter. We have validated our approach with another design: the same procedure is performed in Supplemental Material [29] with a longer and more rigid fish tail; in particular a larger value of γ_c is observed. We note here the square root behavior for the amplitude, which is characteristic of Hopf bifurcations. In Supplemental Material [29], we develop an asymptotic expansion using a small distance to threshold $\gamma - \gamma_c$, and we show:

$$\alpha_0 = \Theta\sqrt{\gamma - \gamma_c}, \tag{10}$$

where $\Theta = 0.97$ rad$^{1/2}$N$^{1/2}$ is predicted from a long expression of the physical parameters given in Supplemental Material [29]. In experiments, Θ is evaluated to $\Theta_{\text{exp}} = 0.72 \pm 0.02$ rad$^{1/2}$N$^{1/2}$ and the agreement is again very satisfactory.

To conclude on the capacity of the proprioceptive loop to induce locomotion, we have submitted the robotic fish to an imposed fixed velocity flow into a water tunnel. As the device is attached to the force sensor, the cruising velocity of the swimmer can be measured by zeroing the value of the longitudinal force F_x with the tuning of the inflow velocity (details in Supplemental Material [29]). In Fig. 5, we show the swimming velocity dependence as a function of the feedback parameter γ. To a first-order approximation, the thrust results from the projection of the normal force to the fin toward the x axis [39]; Assuming a harmonic motion, α and $\dot{\alpha}$ are $\pi/2$ phase-shifted and the term in $\dot{\alpha}$ does not contribute to the thrust; Only added mass effects are relevant and the average thrust equals $\overline{\alpha(t)F_y(t)} \simeq K_{\ddot{\alpha}}\omega^2\alpha_0^2/8 \simeq K_{\ddot{\alpha}}\omega^2\Theta^2(\gamma - \gamma_c)/8$. By balancing the thrust with the typical drag, which is dominated by the pressure drag $C_d\rho U^2 L^2$ (the drag coefficient measured in Supplemental Material [29] equals $C_d \simeq 0.25$, a rather high value that suggests vortex-induced drag is negligible [40]), we determine that the velocity scales as:

$$U \sim \sqrt{\frac{K_{\ddot{\alpha}}}{8C_d\rho L^4}}\omega L\Theta\sqrt{\gamma - \gamma_c} \sim 0.17\sqrt{\gamma - \gamma_c} \tag{11}$$

with SI units, and the order of magnitude of the proportionality constant is in good agreement with that obtained in experiments. This relation is a consequence of the simple force balance and consequently retrieves the constancy of the Strouhal number $\omega L\alpha_0/(2\pi U)$, around 0.3 for swimmers in the turbulent regime [19, 40, 41]. The fact that both α_0 and ω are functions of γ does not modify this balance, so that tuning γ gives a direct control over the swimming velocity.

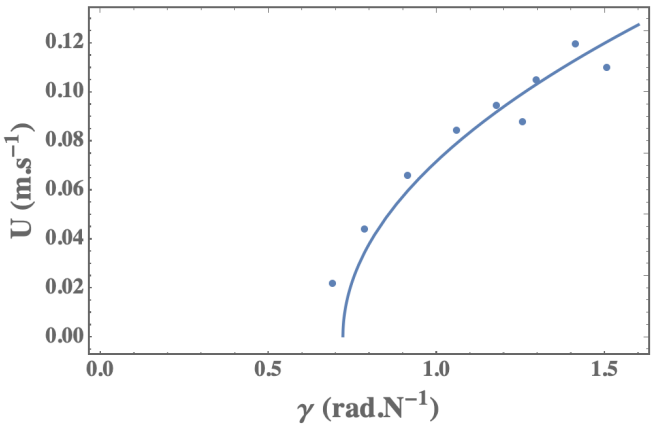

FIG. 5. Swimming velocity U as a function of the proprioceptive feedback parameter γ. The experimental points are shown as disks. The curve represents the fit $U = 0.14\sqrt{\gamma - \gamma_c}$ in SI units.

In this letter, we have proposed a generic model for describing swimming locomotion driven by a proprioceptive loop. Beside the general framework we have introduced, we have developed a simple experiment which enabled us to validate the idea that underwater swimmers might select their amplitude and beating frequency using mechanical sensors. Our simple model permits the realization of a tractable experiment ; beside its simpleness, it is shown to have excellent predictive capabilities.

ACKNOWLEDGMENTS

This work has been supported by the French government, through the UCAJEDI Investments in the Future project managed by the National Research Agency (ANR) with the reference number ANR-15-IDEX-01. François Gallaire is thanked for enlightning discussions and Leo Guschemann for participating in the long tail experiments.

[1] K. Healy, T. H. Ezard, O. R. Jones, R. Salguero-Gómez, and Y. M. Buckley, Animal life history is shaped by the pace of life and the distribution of age-specific mortality and reproduction, Nature ecology & evolution **3**, 1217 (2019).

[2] R. Alexander, *Locomotion of Animals* (Springer Netherlands, 1982).

[3] T. Orlovsky, G. N. Orlovskiĭ, T. Deliagina, and S. Grillner, *Neuronal control of locomotion: from mollusc to man* (Oxford University Press, 1999).

[4] P. A. Guertin, The mammalian central pattern generator for locomotion, Brain research reviews **62**, 45 (2009).

[5] S. Rossignol, R. Dubuc, and J.-P. Gossard, Dynamic sensorimotor interactions in locomotion, Physiological reviews **86**, 89 (2006).

[6] K. G. Pearson, Proprioceptive regulation of locomotion, Current opinion in neurobiology **5**, 786 (1995).

[7] D. Ryczko, S. András, and A. J. Ijspeert, Walking with salamanders: From molecules to biorobotics, Trends in Neurosciences **43**, 916 (2020).

[8] T. Y. Wu, Swimming of a waving plate, Journal of Fluid Mechanics **10**, 321 (1961).

[9] M. J. Lighthill, Aquatic animal propulsion of high hydromechanical efficiency, Journal of Fluid Mechanics **44**, 265 (1970).

[10] J.-Y. Cheng, T. Pedley, and J. Altringham, A continuous dynamic beam model for swimming fish, Philosophical Transactions of the Royal Society of London. Series B: Biological Sciences **353**, 981 (1998).

[11] J. Carling, T. L. Williams, and G. Bowtell, Self-propelled anguilliform swimming: simultaneous solution of the two-dimensional navier-stokes equations and newton's laws of motion, Journal of experimental biology **201**, 3143 (1998).

[12] A. Leroyer and M. Visonneau, Numerical methods for ranse simulations of a self-propelled fish-like body, Journal of Fluids and Structures **20**, 975 (2005).

[13] M. Gazzola, W. M. Van Rees, and P. Koumoutsakos, C-start: optimal start of larval fish, Journal of Fluid Mechanics **698**, 5 (2012).

[14] M. Piñeirua, B. Thiria, and R. Godoy-Diana, Modelling of an actuated elastic swimmer, Journal of Fluid Mechanics **829**, 731 (2017).

[15] R. Williams IV, N. Neubarth, and M. E. Hale, The function of fin rays as proprioceptive sensors in fish, Nature communications **4**, 1 (2013).

[16] M. Gazzola, M. Argentina, and L. Mahadevan, Gait and speed selection in slender inertial swimmers, Proceedings of the National Academy of Sciences **112**, 3874 (2015).

[17] C. L. Hamlet, K. A. Hoffman, E. D. Tytell, and L. J. Fauci, The role of curvature feedback in the energetics and dynamics of lamprey swimming: A closed-loop model, PLoS computational biology **14**, e1006324 (2018).

[18] D. Gross, Y. Roux, and M. Argentina, Curvature-based, time delayed feedback as a means for self-propelled swimming, Journal of Fluids and Structures **86**, 124 (2019).

[19] G. Triantafyllou, M. Triantafyllou, and M. Grosenbaugh, Optimal thrust development in oscillating foils with application to fish propulsion, Journal of Fluids and Structures **7**, 205 (1993).

[20] J. Anderson, K. Streitlien, D. Barrett, and M. Triantafyllou, Oscillating foils of high propulsive efficiency, Journal of Fluid Mechanics **360**, 41 (1998).

[21] C. Rossi, J. Colorado, W. Coral, and a. Barrientos, Bending continuous structures with SMAs: a novel robotic fish design, Bioinspiration & Biomimetics **6**, 045005 (2011).

[22] F. Gibouin, C. Raufaste, Y. Bouret, and M. Argentina, Study of the thrust–drag balance with a swimming robotic fish, Physics of Fluids **30**, 091901 (2018).

[23] J. Zhu, C. White, D. K. Wainwright, V. Di Santo, G. V. Lauder, and H. Bart-Smith, Tuna robotics: A high-frequency experimental platform exploring the performance space of swimming fishes, Science Robotics **4** (2019).

[24] J. Yu, S. Chen, Z. Wu, and W. Wang, On a miniature free-swimming robotic fish with multiple sensors, International Journal of Advanced Robotic Systems **13**, 62 (2016).

[25] A. Ravalli, C. Rossi, and G. Marrazza, Bio-inspired fish robot based on chemical sensors, Sensors and Actuators B: Chemical **239**, 325 (2017).

[26] D. Ji, F. ur Rehman, S. A. Ajwad, K. Shahani, S. Sharma, R. Sutton, S. li, Z. Ye, H. Zhu, and S. Zhu, Design and development of autonomous robotic fish for object detection and tracking, International Journal of Advanced Robotic Systems **17**, 1729881420925284 (2020).

[27] W. Coral, C. Rossi, O. M. Curet, and D. Castro, Design and assessment of a flexible fish robot actuated by shape memory alloys, Bioinspiration & Biomimetics **13**, 056009 (2018).

[28] J. Lee, J. Hwangbo, L. Wellhausen, V. Koltun, and M. Hutter, Learning quadrupedal locomotion over challenging terrain, Science Robotics **5**, 10.1126/scirobotics.abc5986 (2020).

[29] See Supplemental Material at `http://link.aps.org/supplemental/xxx` for videos, the determination of parameters, the long tail analysis and the perturbative approach.

[30] T. Theodorsen, General theory of aerodynamic instability and the mechanism of flutter, Report 496, National Advisory Committee for Aeronautics, Washington DC (1935).

[31] M. Saadat, F.E. Fish, A.G. Domel, V. Di Santo, G.V. Lauder, and H. Haj-Hariri, On the rules for aquatic locomotion, Physical Review Fluids **2**, 083102 (2017).

[32] L. Landau and E. Lifshitz, Theoretical physics, vol. 6, fluid mechanics (1987).

[33] P. A. Dewey, B. M. Boschitsch, K. W. Moored, H. A.

Stone, and A. J. Smits, Scaling laws for the thrust production of flexible pitching panels, Journal of Fluid Mechanics **732**, 29 (2013).

[34] D. B. Quinn, G. V. Lauder, and A. J. Smits, Scaling the propulsive performance of heaving flexible panels, Journal of Fluid Mechanics **738**, 250 (2014).

[35] F. Paraz, C. Eloy, and L. Schouveiler, Experimental study of the response of a flexible plate to a harmonic forcing in a flow, Comptes Rendus Mécanique **342**, 532 (2014).

[36] F. Paraz, L. Schouveiler, and C. Eloy, Thrust generation by a heaving flexible foil: Resonance, nonlinearities, and optimality, Physics of Fluids **28**, 011903 (2016).

[37] J. Sánchez-Rodríguez, C. Raufaste, and M. Argentina, A minimal model of self propelled locomotion, Journal of Fluids and Structures **97**, 103071 (2020).

[38] M. Haragus and G. Iooss, *Local bifurcations, center manifolds, and normal forms in infinite-dimensional dynamical systems* (Springer Science & Business Media, 2010).

[39] I. E. Garrick, Propulsion of a flapping and oscillating airfoil, Report 567, National Advisory Committee for Aeronautics, Washington DC (1936).

[40] D. Gross, Y. Roux, C. Raufaste, and M. Argentina, Drag analysis with a self-propelled flexible swimmer, submitted to Phys. Rev. fluids.

[41] M. Gazzola, M. Argentina, and L. Mahadevan, Scaling macroscopic aquatic locomotion, Nature Physics **10**, 758 (2014).